

Direct band gap opening in graphene by BN doping: *Ab initio* calculationsPrashant P. Shinde^{1,2,*} and Vijay Kumar^{1,†}¹*Dr. Vijay Kumar Foundation, 1969 Sector 4, Gurgaon 122001, Haryana, India*²*Center for Modeling and Simulation, University of Pune, Ganeshkhind, Pune 411007, India*

(Received 5 April 2011; revised manuscript received 20 July 2011; published 1 September 2011)

Ab-initio calculations on graphene doped with boron nitride (BN) nanoribbons and patches show opening of a band gap in all cases. The smallest width of graphene in these hybrid layers controls the band gap that varies slowly around ~ 0.75 eV when the width of graphene region is in the range of 2 to 5 zigzag chains. Most interestingly the band gap is direct in all the cases we have studied and nearly the same for different doping if the smallest graphene width is the same. These results show the possibility of ultrathin hybrid semiconductor graphene with band gap similar to silicon and an additional attractive feature that it is direct.

DOI: [10.1103/PhysRevB.84.125401](https://doi.org/10.1103/PhysRevB.84.125401)

PACS number(s): 73.22.Pr, 61.48.Gh, 71.55.Eq

I. INTRODUCTION

The discovery¹ of graphene has ignited intense research as it has potential to replace silicon for developing possibly the smallest future devices. The electronic band structure of graphene shows linear-energy dispersion near the Fermi energy, and this unique feature is fundamentally responsible for its many interesting properties including high-electron mobility ($\sim 10^5$ cm² V⁻¹ s⁻¹), which is advantageous for achieving high-speed and high-performance next-generation transistors with properties exceeding those of conventional semiconductors. However, graphene lacks a band gap at the Fermi level, which is the defining concept for semiconductors and essential for controlling the conductivity by electronic means. Therefore, band gap engineering of graphene is very important for applications. A hexagonal boron nitride (*h*-BN) layer is isostructural with graphene, and both have nearly the same lattice parameters. However, graphene is metallic with zero band gap at the Dirac Point (K-Point), but *h*-BN layer is a wide band gap semiconductor.² Therefore doping of BN is a natural proposition to develop hybrid graphene with a band gap.

Earlier efforts to open a band gap in graphene have been by hydrogenation³ and adsorption.^{4,5} Hydrogenation of graphene changes its bonding from sp^2 to sp^3 and creates buckling. However, graphene nanoribbons having edges terminated with hydrogen⁶ exhibit band gap due to quantum confinement, but the properties are strongly influenced by the way edges are terminated. Recent experiments⁷ on controlled amount of BN doping in graphene show the possibility of band gap engineering. Such samples have local variations in BN distribution, and it is important to understand the dependence of graphene-electronic structure on different BN configurations. Here, we present results of *ab initio* calculations on BN-doped graphene and show that *the band gaps in seemingly different BN-doped graphene systems have similarity in that the BN-doped graphene systems with nearly the same minimum width of graphene layer between the boundaries of BN patches of different morphologies or ribbons have nearly the same energy band gap*. This finding could help to characterize these hybrid layers for optical and electronic applications.

Monte Carlo simulations on graphene-BN heterostructures have shown⁸ their tendency to phase separate into BN and graphene regions. This study, however, did not consider the

band gap aspect. *Ab initio* calculations on a BC₂N layer⁹ showed alternate zigzag chains of carbon and BN to have lower energy in contrast to a layer with C₂ and BN dimers arranged alternately in an armchair-chain configuration. A small band gap has been predicted from *ab initio* calculations in graphene layer when deposited on a *h*-BN layer,¹⁰ and also gaplike feature of width ~ 126 meV at the Fermi energy has been observed.¹¹ An earlier study¹² of a heterosheet of BNC_x with hexagonal symmetry also found band gap in such structures. Here we study graphene doped with BN in two ways: (1) BN nanoribbons and (2) in the form of BN patches similar to those achieved recently in experiments⁷ and report their atomic and electronic properties by *ab initio* calculations. Our results show opening of a band gap in all cases.

II. METHOD OF CALCULATIONS

The calculations have been performed using projector-augmented-wave pseudopotential-plane-wave method¹³ and generalized gradient approximation¹⁴ (GGA) for the exchange-correlation energy. The cut-off energy for the plane-wave expansion is taken to be 400 eV. The hybrid system is modeled by a 6×6 graphene supercell with 72 (C, B, and N) atoms and 12 Å vacuum space between the layers with periodic boundary conditions. The shape and size of the 2D supercell and the atomic positions are optimized using the Γ -point until the force on each ion becomes less than 0.005 eV/Å and the energy is converged within 0.0001 eV. The cohesive energy has been calculated from $E = (-E_{\text{CBN}} + N_{\text{C}}E_{\text{C}} + N_{\text{B}}E_{\text{B}} + N_{\text{N}}E_{\text{N}})/N_{\text{at}}$, where E_{CBN} , E_{C} , E_{B} , and E_{N} are the total energies of the combined C-BN system, free C, B, and N atoms, respectively, and N_{C} , N_{B} , and N_{N} are the number of C, B, and N atoms, respectively, in the supercell, while N_{at} is the total number of atoms in the supercell. The electronic density of states (DOS) has been calculated using $15 \times 15 \times 1$ \mathbf{k} -points in the Brillouin zone of the supercell. Further tests have been performed in some of the cases with spin polarization as there are reports^{15,16} of magnetism at BN-C interface in zigzag nanoribbons. Also we considered a large vacuum space of 22 Å in the supercell of BN-doped graphene layers. However, we did not find any significant difference in energy as well as band gap. The Brillouin zone of a primitive unit cell of graphene with reciprocal lattice vectors \mathbf{b}_1 and \mathbf{b}_2

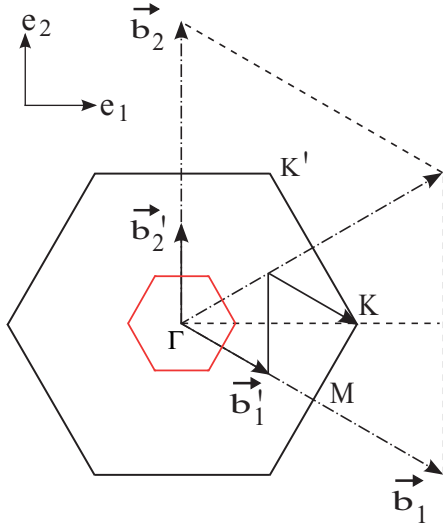


FIG. 1. (Color online) Brillouin zone (outer hexagon) of a primitive unit cell of graphene with reciprocal lattice vectors \mathbf{b}_1 and \mathbf{b}_2 . Γ , K , K' , and M show the symmetry \mathbf{k} -points in the Brillouin zone. The inner hexagon is the Brillouin zone of a graphene supercell with edges three times the edge length of a primitive graphene unit cell. The reciprocal lattice vectors \mathbf{b}_1' and \mathbf{b}_2' of the supercell are related to \mathbf{b}_1 and \mathbf{b}_2 with $\mathbf{b}_1' = \mathbf{b}_1/3$ and $\mathbf{b}_2' = \mathbf{b}_2/3$. Interestingly in this case and in all cases with the supercell sides being integer multiple of three ($3m$, m , an integer), the Γ -point and the K -point corresponding to the primitive graphene unit cell coincide. One can see that the K -point of the primitive unit cell can be reached from Γ -point with $2\mathbf{b}_1' + \mathbf{b}_2'$ translation. \mathbf{e}_1 and \mathbf{e}_2 are the unit vectors along x and y directions.

is shown in Fig. 1, and the symmetry points Γ , K , K' , and M have been marked. Interestingly for a graphene *supercell* with the cell dimensions being an integer multiple of three ($3m$, m , an integer), the Γ -point and the K -point of the primitive graphene unit cell become the same, as shown in Fig. 1 for $m = 1$ case. The reciprocal lattice vectors of the supercell are $\mathbf{b}_1' = \mathbf{b}_1/3$ and $\mathbf{b}_2' = \mathbf{b}_2/3$. Therefore, the Dirac-point feature observed at K -point of the primitive unit cell can be expected to show up at the Γ -point for the supercell in our case of $m = 2$. The character of the M -point remains similar in the supercell Brillouin zone.

III. RESULTS

The atomic structures of a graphene and a *h*-BN layer are shown in Figs. 2(a) and (d), respectively. The calculated cohesive energy, 7.95 eV/atom, of graphene is higher than 7.12 eV/atom for a *h*-BN layer. The large values in both the cases reflect their strong stability. The calculated B-N bond length (1.45 Å) compares well with the experimental result (1.44 ± 0.1) in Ref. 17 and 1.45 Å in an earlier calculation in Ref. 18. The C-C bond length in graphene is 1.42 Å. Therefore, the mismatch in B-N and C-C bond lengths is small. The calculated band gap of a *h*-BN layer is 4.53 eV and is in agreement with 4.66 eV calculated in an earlier work,² but it is smaller than 5.97 eV obtained from experiments¹⁹ on bulk *h*-BN due to underestimation by GGA.

Figure 2 shows all the studied nanoribbons and *h*-BN patches of different sizes and shapes in graphene. The cohesive

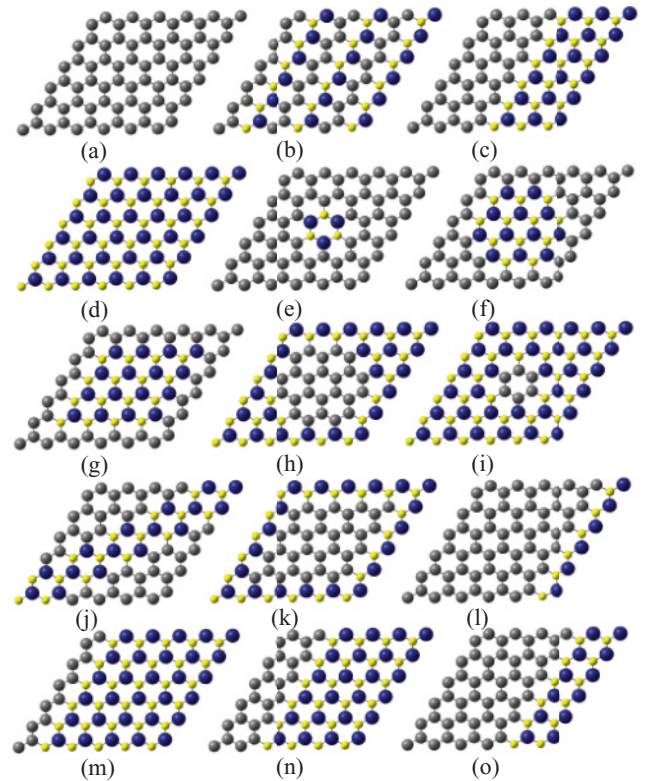


FIG. 2. (Color online) Atomic structures with different distributions of C, B, and N atoms in the supercell. (a) Pure graphene, (b) alternate zigzag chains of C and BN, (c) nanoribbons of graphene and *h*-BN each with three chains, (d) pure *h*-BN layer, (e) a BN hexagon in graphene supercell, (f) a *h*-BN patch with seven hexagons in graphene supercell, (g) a *h*-BN patch with a crossed graphene mesh, (h) graphene patch with seven hexagons in a *h*-BN layer, (i) a quantum dot of graphene in *h*-BN, (j) a BN nanoribbon along the diagonal of the supercell, (k) a graphene patch with crossed-BN mesh, (l) graphene with a BN-zigzag chains, (m) one zigzag chain of carbon and five chains of BN (C1BN5), (n) two zigzag chains of C and four chains of BN (C2BN4), and (o) four chains of carbon and two chains of BN (C4BN2). Large (blue), medium (grey), and small (yellow) balls represent N, C, and B atoms, respectively.

energy of the hybrid layers lies in between the values for a graphene and a *h*-BN layer, as shown in the inset in Fig. 3(a). When graphene is patterned into a narrow nanoribbon bounded by *h*-BN regions, the charge carriers are confined in to a quasi-one-dimensional (1D) system, and an energy gap could open up due to quantum confinement. This is expected to depend on the width and crystallographic orientation of the graphene nanoribbon.²⁰

Figure 2(b) shows a layer with alternate C- and BN-zigzag chains. It does not have the lowest energy, and a configuration with alternate zigzag nanoribbons of C and *h*-BN, each with three chains [Fig. 2(c)] within the supercell, is 9.62 eV lower in energy, supporting earlier results of phase separation.⁸ The B-C and N-C bond energies are less favorable compared with C-C bonds, and fewer C-BN interfaces in Fig. 2(c) lower the energy of this configuration. As the number of BN chains n is increased from one to five in *h*-BN nanoribbons, the cohesive energy decreases [Fig. 3(a)]. Figure 2(j) shows an armchair

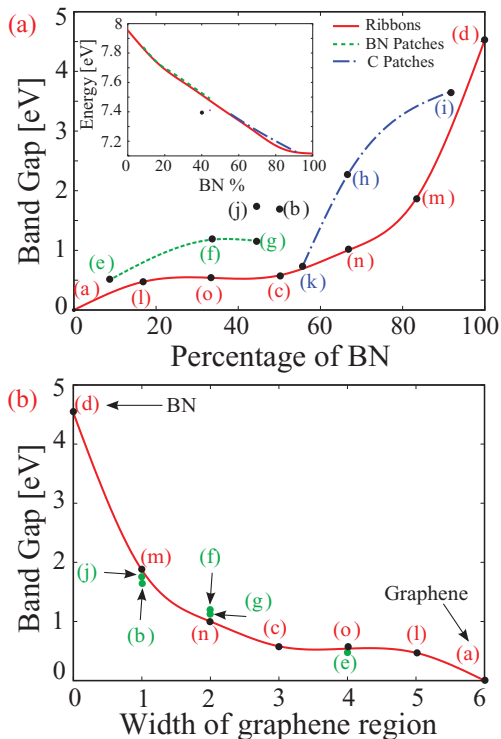


FIG. 3. (Color online) (a) Energy band gap for different configurations of BN-doped hybrid graphene in the supercell, as given in Fig. 2. The points have been connected to aid the eye and show the trend. Full line, broken line, and dash-dot line correspond to BN-zigzag nanoribbons, BN patches in graphene, and graphene patches in h -BN. The dots (b) and (j) correspond to alternate BN and C chains in the unit cell, as shown in Fig. 2(b), and an armchair BN nanoribbon in graphene as shown in Fig. 2(j), respectively. The points (a), (c), (d), (l), (m), (n), and (o) on the full line correspond to BN-zigzag nanoribbons as shown in Fig. 2. Inset shows the corresponding cohesive energy per atom. (b) Energy band gap variation with the width of the smallest graphene region bounded by BN in different doping cases as shown in Fig. 2. Points on the curve [(a), (c), (d), (l), (m), (n), (o)] indicate BN-zigzag nanoribbons, whereas the remaining points (green) indicate other cases with similar band gaps as that of nanoribbons.

h -BN nanoribbon along the diagonal of the graphene supercell, and it is ~ 5.7 eV higher in energy as compared to a BN patch surrounded by C-mesh, as shown in Fig. 2(g) with the same BN concentration. This is again due to less number of unfavorable B-C and N-C bonds in Fig. 2(g). However, the configuration in Fig. 2(c) has lower energy than the one in Fig. 2(j) even though the BN fraction in Fig. 2(c) is 50% compared with 44.45% in Fig. 2(j), because the BN distribution in Fig. 2(j) leads to a larger number of unfavorable B-C and N-C pairs. These results suggest that in such hybrid systems, minimization of B-C and N-C bonds would lead to energetically favorable configurations. However, as C-C and B-N bonds are strong, metastable structures can be expected to also be stable.

When the number of BN chains becomes larger than that of the carbon chains in the supercell, we can consider the hybrid system as a h -BN layer doped with C nanoribbons. Figure 3(a) and Table I give the band gap and the cohesive

TABLE I. The total cohesive energy per supercell, cohesive energy per atom, direct (D) band gap for different amount of BN doping in graphene supercell.

System	BN%	Total cohesive energy/supercell [eV]	Cohesive energy/atom [eV]	Band gap [eV]
(a)	0.00	572.73	7.95	0.00 (at Γ)
(b)	50.00	525.09	7.29	1.65 (D at Γ)
(c)	50.00	534.71	7.43	0.58 (D at M)
(d)	100.00	512.35	7.12	4.53 (D at Γ)
(e)	8.33	564.58	7.84	0.49 (D at Γ)
(f)	33.67	545.97	7.58	1.18 (D at Γ)
(g)	44.45	539.24	7.49	1.16 (D at Γ)
(h)	66.67	525.37	7.30	2.27 (D at Γ)
(i)	91.67	517.85	7.19	3.66 (D at Γ)
(j)	44.45	533.54	7.41	1.74 (D at Γ)
(k)	55.56	528.76	7.34	0.72 (D at Γ)
(l)	16.67	556.21	7.73	0.47 (D near Γ)
(m)	83.33	514.83	7.15	1.86 (D at Γ)
(n)	66.67	524.44	7.28	1.00 (D near M)
(o)	33.33	545.28	7.57	0.54 (D near M)

energy as a function of the percentage of BN, while in Fig. 3(b) the band gap is given as a function of the minimum width of the graphene region. In the cases of the nanoribbons the C-BN interface remains unchanged and the cohesive energy decreases nearly linearly [inset in Fig. 3(a)] as the width of the BN nanoribbon increases. Figures 2(c), (l), and (o) represent hybrid layers with three to five graphene zigzag chains in the supercell for which the energy band gap [Fig. 3(a)] remains nearly flat. Increasing the number of BN chains leads to a rapid rise in the band gap toward the value for a h -BN layer. The quantum-confinement effects increase when the width of the graphene nanoribbon decreases, and it leads to an increase in the band gap [Fig. 3(b)], which is direct in all these cases. Our results agree with those obtained earlier for 2D superlattices of C and BN zigzag nanoribbons.¹⁵ The electronic states near the Fermi level in the hybrid graphene layers get significantly modified with the opening of a gap, as shown in Fig. 4. We also checked the effect of spin polarization on the band gap in such nanoribbons. However, we did not find any magnetic solution for the case of nanoribbons. This agrees with the earlier results¹⁵ where spin-polarization effects were reported to occur in those cases where the total number of zigzag chains (C plus BN) in the supercell exceeded eight.

An interesting point to be noted here is that for supercells with the lattice vectors \mathbf{a}_1' and \mathbf{a}_2' multiples of 3 ($3m$, m , an integer) of the unit cell vectors of pure graphene, the Γ -point and K-point of the primitive cell become identical (Fig. 1), and therefore, the band crossing as well as band gap opening is expected to occur at the Γ -point for our supercell with $m = 2$. For the case of small band gap at the Γ -point of the supercell, nearly linear dispersion can be seen slightly away from the Γ -point as in Fig. 4(e). The direct band gap opening at the Γ -point has also been reported in hybrid graphene-BN structures by Xu *et al.*²¹ who considered a 9×9 supercell, which is also a multiple of three. An interesting observation is that the band gap for a zigzag carbon chain in the supercell

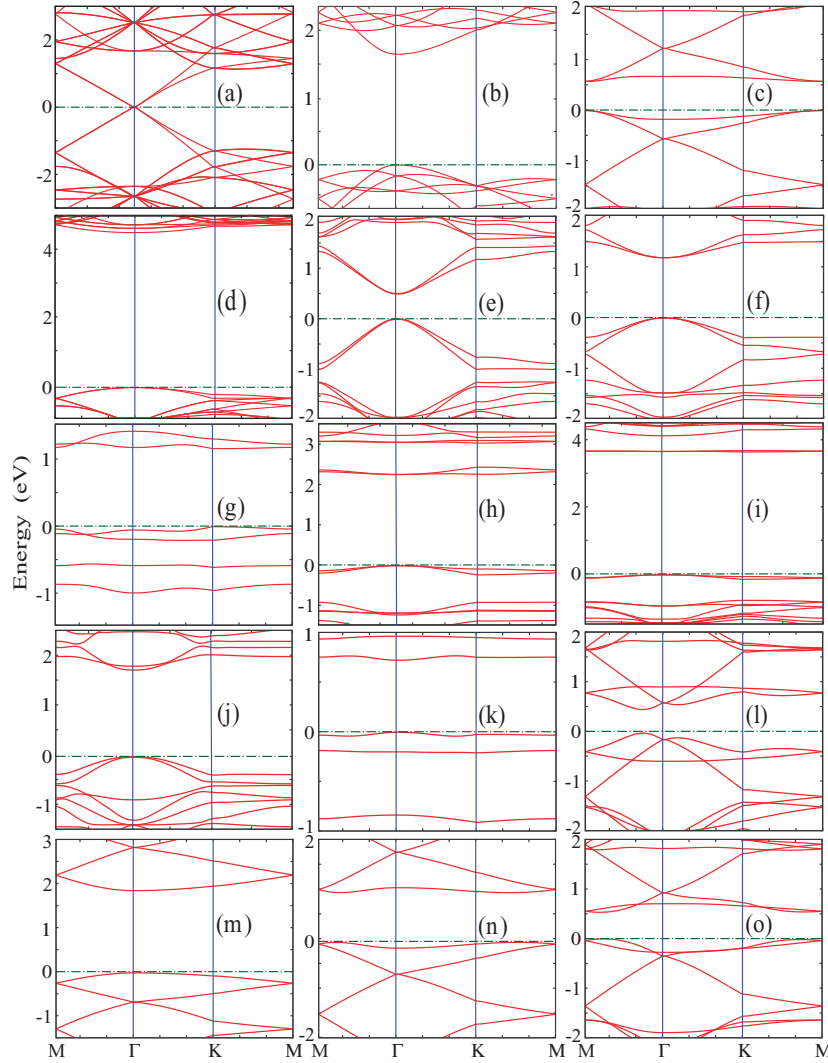


FIG. 4. (Color online) Energy bands along symmetry directions of the Brillouin zone of the supercell corresponding to the atomic structures shown in Fig. 2. The dashed line shows the top of the valence band.

of h -BN layer (1.86 eV) is nearly the same as in the case of Fig. 2(b) (1.65 eV) where a zigzag carbon chain is bounded by one BN chain on either side. The latter case has been reported in Ref. 2, and our band gap value agrees well with their calculated value of 1.66 eV. These results suggest that one chain of BN on either side of a carbon nanoribbon may produce major effects of quantum confinement.

In experiments on h -BN doped graphene-hybrid layers, graphene and BN regions are separate⁷ (h -BN patches in graphene) and often there are two or three atomic layers but also regions of single-layer thickness. We focus on the modifications in the electronic structure of a single-layer graphene by doping different shapes of BN patches [Figs. 2(e)–(g)] keeping B and N concentrations equal. The cohesive energy per atom and the band gap are shown in Fig. 3(a). A BN hexagon (quantum dot) at the center of the graphene supercell increases the energy of the system by 8.15 eV and causes a *direct* band gap opening of 0.49 eV at the Γ -point. In this case we find that the spin-polarized calculations lead to a solution that is about 0.1 eV lower in energy as compared to the non-spin polarized solution, but there is no significant difference in the band gap value. The spin polarization is very small with the down-spin polarization more around the B-C

bond, while the up-spin polarization is more diffused with the distribution around B, C, and N atoms. With an increase in the patch size, the C-BN interface increases [Fig. 2(f) for seven BN hexagons], and it increases the direct band gap at the Γ -point to 1.18 eV due to the narrowing of the graphene region. In this case the smallest width of the graphene region between the BN patches is two chains and strikingly the band gap of a h -BN layer doped with a graphene nanoribbon of two zigzag chains is nearly the same (1.00 eV), as shown in Fig. 3 marked with (n) for $(\text{BN})_4\text{C}_2$. Furthermore, in this case spin-polarized calculations did not give any change in energy or band gap. It is also striking that for a slightly bigger BN patch [Fig. 2(g)] but with the same width of crossed graphene nanoribbons having two zigzag chains, the band gap is very nearly the same (1.16 eV), though the distribution and concentration of BN in the two cases are different. A similar behavior is obtained for the configuration in Fig. 2(e) where the minimum width of the graphene region is four chains. Its band gap (0.49 eV) is quite close to the value (0.54 eV) for graphene and BN nanoribbons with four carbon and two BN-zigzag chains, respectively, in the supercell [case $(\text{BN})_2\text{C}_4$ in Fig. 3 marked with (o)]. *These results suggest the importance of the narrowest region of graphene for the band gap of the hybrid structures.* Our results

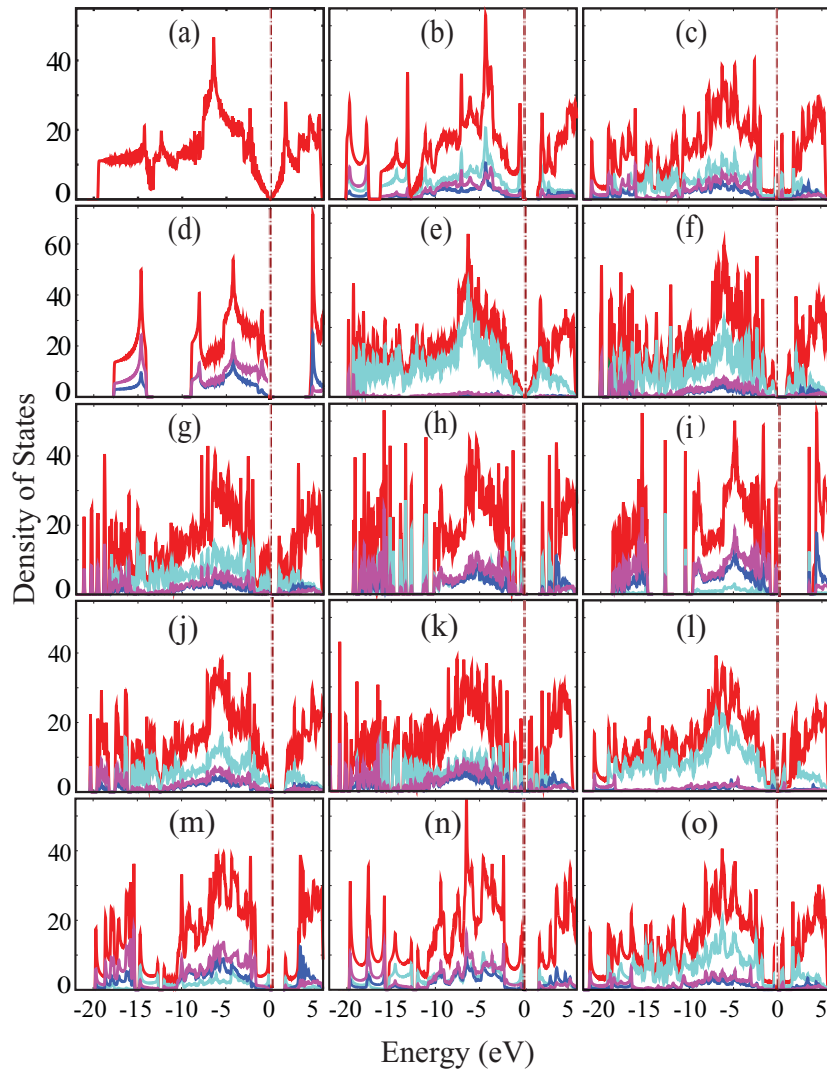


FIG. 5. (Color online) The total and partial DOS corresponding to the atomic structures in Fig. 2 obtained by using Gaussian broadening of 0.05 eV. Light blue (light grey), pink (grey), and blue (darker grey) curves show C, B, and N contributions. Red (darkest grey) curves represent the total density of states. Vertical dashed dotted line is the top of the valence band.

of the band gap are given in Fig. 3(b) as a function of the width of the narrowest region of graphene in the supercell. Further, it is seen that for a given concentration of BN such as $\sim 33\%$ (see Table I), the patch configuration is more favorable than the nanoribbon configuration due to less number of unfavorable C-B and C-N bonds. In the reverse case [Fig. 2(k)] of a graphene patch (quantum dot) totally covered by crossed BN-zigzag nanoribbons (mesh), the structure is energetically less favorable compared with a *h*-BN patch covered by graphene [Fig. 2(g)] due to higher atomic fraction of BN. The band gap in this case is 0.44 eV smaller compared with the value for Fig. 2(g) due to wider width of graphene patch (four chains) though quantum confinement in both the directions increases the gap from 0.54 eV for the case of (o) of four infinite graphene chains to 0.72 eV for the graphene quantum dot. Further reduction in the size of the graphene patch, as shown in Figs. 2(h) and (i), leads to a sharp increase in the band gap towards the value of a *h*-BN layer [see Fig. 3(a) and Table I].

The formation of C-BN interface in hybrid layers leads to a small variation in the interatomic distances and to a lesser extent in the lattice parameter of graphene. In general the C-B bond length in different structures is the largest (1.48–1.52 Å), while C-N bonds lie in the range of 1.37 to 1.41 Å. The

C-C bonds (1.39–1.44 Å) have a slight contraction as well as expansion (near the interface) compared with the value for pure graphene. Below we discuss the electronic band structure of the hybrid layers with approximately equal magnitude of \mathbf{a}_1' and \mathbf{a}_2' vectors using Γ -, K-, M-, and X-points in the Brillouin zone of the supercell.

The band structures for different BN-doped graphene layers show (Fig. 4) that there is an opening of a band gap in all cases. BN doping removes the equivalence of two interpenetrating sublattices in graphene and induces a band gap, as in the case of a *h*-BN layer. For zigzag nanoribbons [Figs. 2(b) and 2(c)] the band gap is direct at Γ - and M-point, respectively. In other cases, such as one zigzag-BN chain in graphene, the direct band gap is at a \mathbf{k} -point in between M and Γ [Fig. 4(l)]. For the different BN patches in graphene, there is a direct band gap either at Γ - or M-point (Table I). The GGA value of the band gap for the hybrid structures in Figs. 2(e)–2(g) lies in the range of 0.49–1.18 eV. As the band gap is underestimated in GGA, the actual value of the band gap is expected to be larger and close to the value for silicon in some cases. Therefore *such BN-doped graphene layers offer an interesting possibility for nanoelectronics with direct band gap that has nearly the same value as in bulk silicon.*

The total and the partial DOS for different BN-doped graphene layers are shown in Fig. 5 together with those of the pure graphene and a *h*-BN layer [Figs. 5(a) and 5(d), respectively]. For alternate C- and BN-zigzag chains [Fig. 5(b)], the DOS shows features that are a combination of those of pure graphene and a *h*-BN layer because of the equal composition of C and BN. The sharp features in the DOS are reflections of the 1D nature of this system. For C and BN nanoribbons, each with three chains, the sharp features seen in Fig. 5(b) become weaker and the band gap is also smaller [Fig. 5(c)] due to an increase in the width of the graphene nanoribbon. In other cases where the BN concentration is low, such as in Figs. 5(e) and 5(f), the DOS at the top of the valence band and the bottom of the conduction band has admixture of both C and BN characters, but carbon contribution is most dominant and therefore contribution to electronic conduction will be from graphene. As the size of the BN patch increases, its contribution to DOS at the top of the valence band and the bottom of the conduction band increases, as shown in Fig. 5(g), for graphene mesh and BN patch. For a graphene quantum dot in *h*-BN [Figs. 5(h) and 5(i)], the DOS shows some sharp peaks in the energy range between approximately -10 to -15 eV, where pure *h*-BN does not have any states. Therefore these states are the energy levels of the small graphene QD. There is also a sharp peak just below the Fermi energy.

IV. SUMMARY

In summary *ab initio* calculations show that a variable band gap is created in graphene by BN doping leading to the possibility of band gap engineering. In all cases we have studied, the band gap is direct, and this could lead to applications of hybrid graphene layers in optoelectronics and solar cells. An important finding is that the band gap depends upon the narrowest region of graphene irrespective of the concentration and shape of BN patches. This result should help in tailoring the band gap of such hybrid layers. Further we find that for the narrowest regions of graphene with 2 to 5 zigzag-C chains, the band gap varies slowly around the GGA value of about 0.75 eV. Therefore keeping the distribution of BN such as to create narrowest regions of graphene in this size range, it could be possible to have band gap with a value similar to that of bulk silicon but with an added significant advantage of being direct. We hope our results will stimulate further experiments on the electronic structure of these systems as well as their applications.

We gratefully acknowledge discussions with P. Ajayan and partial financial support from the Asian Office of Aerospace Research and Development (AOARD). We are thankful to the staff of the Center for Development of Advanced Computing (CDAC) for the supercomputer resources and their excellent support.

*Present address: Dr. Vijay Kumar Foundation.

†kumar@vkf.in

¹K. S. Novoselov, A. K. Geim, S. V. Morozov, D. Jiang, Y. Zhang, S. V. Dubonos, I. V. Grigorieva, and A. A. Firsov, *Science* **306**, 666 (2004).

²F. W. Averill, J. R. Morris, and V. R. Cooper, *Phys. Rev. B* **80**, 195411 (2009).

³D. Haberer, D. V. Vyalikh, S. Taioli, B. Dora, M. Farjam, J. Fink, D. Marchenko, T. Pichler, O. K. Ziegler, S. Simonucci, M. S. Dresselhaus, M. Knupfer, B. Büchner, and A. Grüneis, *Nano Lett.* **10**, 3360 (2010).

⁴S. Niyogi, E. Bekyarova, M. E. Itkis, H. Zhang, K. Shepperd, J. Hicks, M. Sprinkle, C. Berger, C. N. Lau, W. A. deHeer, E. H. Conrad, and R. C. Haddon, *Nano Lett.* **10**, 4061 (2010).

⁵D. A. Abanin, A. V. Shytov, and L. S. Levitov, *PRL* **105**, 086802 (2010).

⁶S. Bhandary, O. Eriksson, B. Sanyal, and M. I. Katsnelson, *Phys. Rev. B* **82**, 165405 (2010).

⁷L. Ci, L. Song, C. Jin, D. Jariwala, D. Wu, Y. Li, A. Srivastava, Z. F. Wang, K. Storr, L. Balicas, F. Liu, and P. M. Ajayan, *Nat. Mater.* **9**, 430 (2010).

⁸K. Yuge, *Phys. Rev. B* **79**, 144109 (2009).

⁹A. Y. Liu, R. M. Wentzcovitch, and M. L. Cohen, *Phys. Rev. B* **39**, 1760 (1989).

¹⁰G. Giovannetti, P. A. Khomyakov, G. Brocks, P. J. Kelly, and J. van den Brink, *Phys. Rev. B* **76**, 073103 (2007).

¹¹R. Decker, Y. Wang, V. W. Brar, W. Regan, H.-Z. Tsai, Q. Wu, W. Gannett, A. Zettl, and M. F. Crommie, *Nano Lett.* **11**, 2291 (2011).

¹²S. Okada, M. Igami, K. Nakada, and A. Oshiyama, *Phys. Rev. B* **62**, 9896 (2000).

¹³G. Kresse and D. Joubert, *Phys. Rev. B* **59**, 1758 (1999); P. E. Blochl, *ibid.* **50**, 17953 (1994).

¹⁴J. P. Perdew, in *Electronic Structure of Solids '91*, edited by P. Ziesche and H. Eschrig (Akademie, Berlin, 1991) p. 11.

¹⁵J. M. Pruneda, *Phys. Rev. B* **81**, 161409 (2010).

¹⁶Y. Ding, Y. Wang, and J. Ni, *Appl. Phys. Lett.* **95**, 123105 (2009).

¹⁷C. Jin, F. Lin, K. Suenaga, and S. Iijima, *Phys. Rev. Lett.* **102**, 195505 (2009).

¹⁸Y.-H. Kim, K. J. Chang, and S. G. Louie, *Phys. Rev. B* **63**, 205408 (2001).

¹⁹K. Watanabe, T. Taniguchi, and H. Kanda, *Nat. Mater.* **3**, 1134 (2004).

²⁰Y.-W. Son, M. L. Cohen, and S. G. Louie, *Phys. Rev. Lett.* **97**, 216803, (2006); M. Y. Han, B. Özyilmaz, Y. Zhang, and P. Kim, *ibid.* **98**, 206805 (2007).

²¹B. Xu, Y. H. Lu, Y. P. Feng, and J. Y. Lin, *J. Appl. Phys.* **108**, 073711 (2010).